Cross-Saturation Effects in IPM Motors and Related Impact on Sensorless Control

Paolo Guglielmi, Michele Pastorelli, *Member, IEEE*, and Alfredo Vagati, *Fellow, IEEE*

***Abstract*—Permanent-magnet-assisted synchronous reluctance motors are well suited to zero-speed sensorless control because of their inherently salient behavior. However, the cross-saturation effect can lead to large errors on the position estimate, which is based on the differential anisotropy. These errors are quantified in this paper as a function of the working point. The errors that are calculated are then found to be in good accordance with the purposely obtained experimental measurements.**

***Index Terms*—Cross-saturation effect, permanent-magnet-assisted synchronous reluctance (PMASR) motor, sensorless ac drives, sensorless control.**

I. Introduction

THE MANY advantages of sensorless ac drives are well recognized. The lower cost, the reduced motor size, the elimination of sensor cabling, and the increased reliability are extending sensorless technology to a wider and wider class of practical applications.

Although the methods based on fundamental excitation of the machine [e.g., generated back electromotive force (EMF)] are still appropriate for specific drive applications, the interest has been focused in the last decade on those methods that are suitable for very low speed and zero speed. This extends the sensorless technology to various types of low-resolution position control, as well as to those cases of speed control, where an extremely high accuracy is wanted (e.g., in the textile industry).

The methods suited to position control are generally based on deterministic spatial saliencies and require some kind of persistent excitation, at least at low speed [23], [24]. Many kinds of excitation are proposed in the literature, including various types of carrier signals and modified pulsewidth-modulated [1], [6], [11], [15] patterns. Rotating vectors [2], [17], [18] are adopted, as well as stationary (pulsating) vectors [12], [13], [22] and common-mode signals [21]. Both voltage [2], [13], [17], [18], [22] and current [12], [16] are used as injected signals.

On the other hand, the availability of a position signal and the need for a deterministic saliency can shift the attention from induction motors to motors of the synchronous type naturally exhibiting a salient behavior, i.e., synchronous reluctance (SyR), permanent-magnet-assisted synchronous reluctance (PMASR) motors, and interior permanent-magnet (IPM) motors.

In fact, the zero-speed sensorless control of induction motors can require purposely engineered saliencies such as those described in [23]. The effect of rotor slots can also be used at that aim [15], [18], although this effect is strongly reduced by rotor skewing. On the contrary, IPM, PMASR, and SyR motors are inherently salient and do not require any design modification, in general. Moreover, they show a better efficiency. Thus, a larger use of these motors is expected for sensorless applications in the next future. However, the flux-versus-current relationships of IPM, PMASR, and SyR motors are far from linear, and saturation and cross saturation heavily affect the motor anisotropy. This has a relevant impact on the detection of rotor position through signal injections of any kind, which represents the only way to obtain reliable position estimates at low speed and zero speed.

The aim of this paper is to point out and quantify the large errors that are introduced in the standard sensorless control schemes by the cross-saturation phenomenon. Reference is made to those schemes based on sinusoidal signal injection of both rotating and pulsating types.

An analytical approach is presented first, leading to a quantitative evaluation of the introduced orientation error, which depends on the motor working point. Then, experimental results are given, confirming the accuracy of the previous analysis and the need for an accurate compensation of the cross-saturation impact, as proposed in [25].

II. Differential Magnetic Behavior and Sensorless Orientation Error

The rotor section of a four-barrier-per-pole IPM motor is shown in Fig. 1. The permanent-magnet (PM) material (i.e., NdFeB) is evidenced (dark area). Let us refer to the rotor (d, q) frame shown in Fig. 1, where the d-axis is chosen in the direction of maximum permeance, as usual, when dealing with SyR motors. As a consequence, the PM flux will be in the $(-q)$ direction. This choice is opportune when the PM flux is limited and the IPM machine is a PMASR. In Figs. 2–5, the flux-versus-current characteristics are reported of an existing IPM (PMASR) machine (Fig. 1). These characteristics are symmetrical with respect to the d-axis, while the symmetry is lost with respect to the q-axis because of the PM polarization. From the figures, the nonlinear magnetic behavior is evident. In particular, a very relevant cross-saturation effect is pointed out. Both the d and q current components span from 0 to 30 A to give

Paper IPCSD-06-065, presented at the 2005 Industry Applications Society Annual Meeting, Hong Kong, October 2–6, and approved for publication in the IEEE Transactions on Industry Applications by the Industrial Drives Committee of the IEEE Industry Applications Society. Manuscript submitted for review October 15, 2005 and released for publication July 6, 2006.

The authors are with the Dipartimento di Ingegneria Elettrica, Politecnico di Torino, 10129 Torino, Italy (e-mail: paolo.guglielmi@polito.it; michele.pastorelli@polito.it; alfredo.vagati@polito.it).

Digital Object Identifier 10.1109/TIA.2006.882646

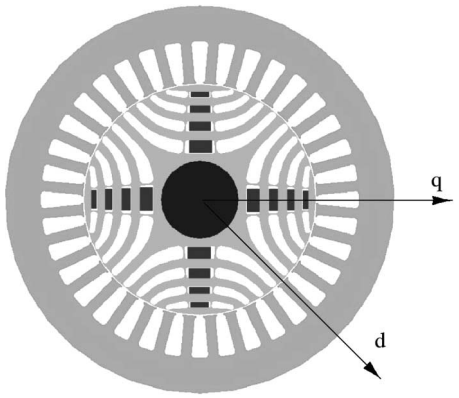

Fig. 1. Four-pole IPM motor and considered reference frame.

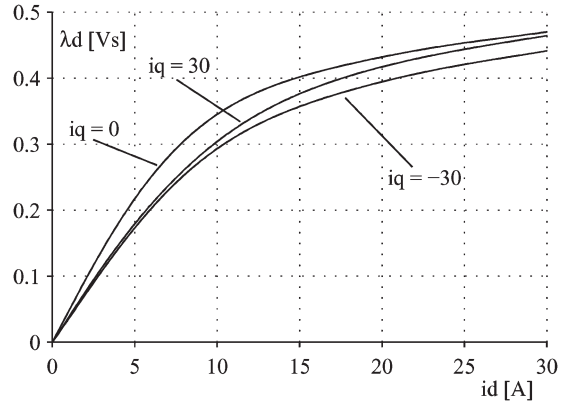

Fig. 2. Measured flux-versus-current characteristic $\lambda_d = \lambda_d(i_d, i_q)$. Parameter values: $i_q = -30$, 0, and 30 A.

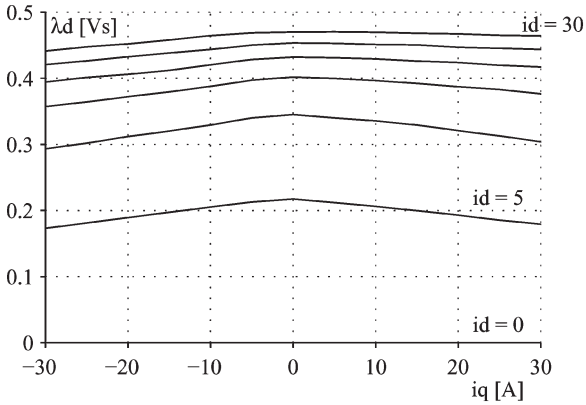

Fig. 3. Measured flux-versus-current characteristic $\lambda_d = \lambda_d(i_d, i_q)$. Parameter values: $i_d = 0, 5, 10, 15, 20, 25$, and 30 A.

evidence to the nonlinear behavior in the whole plane, although negative q current values do not have a practical interest. The rated current amplitude is near to 20 A (peak).

To analyze the impact of cross saturation on sensorless control, a small-signal linearized model has to be considered because of the small flux and current oscillations at the injected carrier frequency. From the general relationship, i.e.,

$$\begin{cases} \lambda_d = \lambda_d(i_d, i_q), \\ \lambda_q = \lambda_q(i_d, i_q), \end{cases} \quad \frac{\partial \lambda_d}{\partial i_q} = \frac{\partial \lambda_q}{\partial i_d} = l_{dq} \tag{1}$$

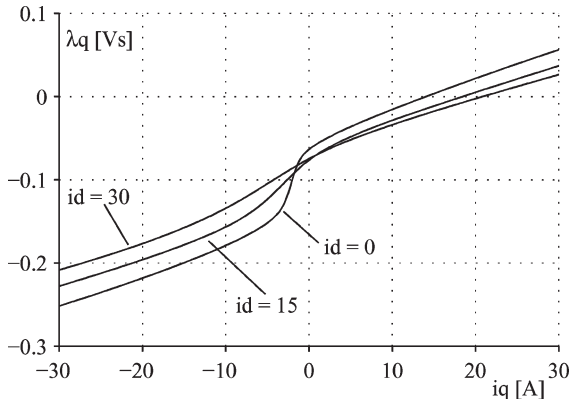

Fig. 4. Measured flux-versus-current characteristic $\lambda_q = \lambda_q(i_d, i_q)$. Parameter values: $i_d = 0$, 15, and 30 A.

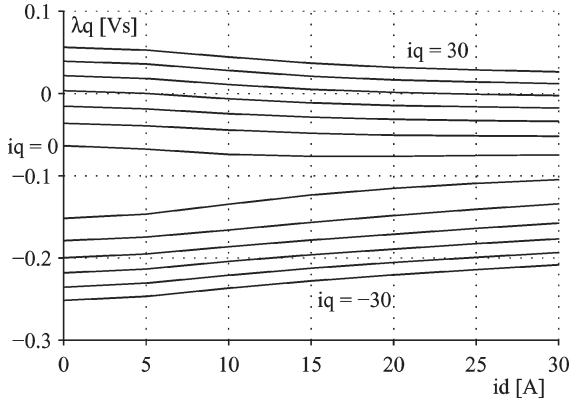

Fig. 5. Measured flux-versus-current characteristic $\lambda_q = \lambda_q(i_d, i_q)$. Parameter values: i_q from -30 to 30 A (step interval: 5 A).

the linearized model is then obtained, i.e.,

$$\delta\lambda_{dq} = \begin{vmatrix} l_d & l_{dq} \\ l_{dq} & l_q \end{vmatrix} \delta i_{dq} \tag{2}$$

giving evidence to the differential inductances l_d, l_q, and l_{dq}. The shown transversality condition imposes the symmetry of the small-signal inductance matrix in (2).

The symbols δi_{dq} and $\delta\lambda_{dq}$ stand for small-signal current and flux vectors, respectively, as well as the column matrices in (2). By using the complex notation and introducing the complex conjugate current $\delta i'_{dq} = \delta i_d - j\delta i_q$, (2) can be rewritten as

$$\delta\lambda_{dq} = \frac{l_d + l_q}{2}\delta i_{dq} + \left(\frac{l_d - l_q}{2} + j l_{dq}\right)\delta i'_{dq} \tag{3}$$

where the positive and negative sequence components are evidenced.

Because of the cross-saturation inductance l_{dq}, the negative sequence component is rotated by the angle ε, i.e.,

$$\varepsilon = \arctan\frac{2l_{dq}}{l_d - l_q}. \tag{4}$$

Since a flux (voltage) vector is more commonly imposed, reference is made to the inverse relationship, i.e.,

$$\begin{cases} \delta i_{dq} = \frac{l_d+l_q}{2\Delta}\delta\lambda_{dq} - \left(\frac{l_d-l_q}{2\Delta} + j\frac{l_{dq}}{\Delta}\right)\delta\lambda'_{dq} \\ \Delta = l_d l_q - l_{dq}^2. \end{cases} \tag{5}$$

In the literature, (5) is more frequently written on the stationary frame (α, β). Due to (6), (7) is obtained from (5) on that frame, i.e.,

$$\delta i_{dq} = e^{-j\vartheta}\delta i_{\alpha\beta};\ \delta\lambda_{dq} = e^{-j\vartheta}\delta\lambda_{\alpha\beta};\ \delta\lambda'_{dq} = e^{+j\vartheta}\delta\lambda'_{\alpha\beta} \tag{6}$$

$$\delta i_{\alpha\beta} = \frac{l_d+l_q}{2\Delta}\delta\lambda_{\alpha\beta} - \left(\frac{l_d-l_q}{2\Delta} + j\frac{l_{dq}}{\Delta}\right)e^{2j\vartheta}\cdot\delta\lambda'_{\alpha\beta}. \tag{7}$$

Of course, the negative sequence component in (7), which contains the rotor position information, is still rotated by the angle ε given in (4). When a rotating voltage vector $\delta v_{\alpha\beta}$ is applied at a carrier pulsation ω_c, (8) can be written and (9) is obtained, i.e.,

$$\begin{aligned} \delta v_{\alpha\beta} &= \delta v \cdot e^{j\left(\omega_c t + \frac{\pi}{2}\right)} \\ \delta\lambda_{\alpha\beta} &\cong \frac{\delta v}{\omega_c}e^{j\omega_c t};\ \delta\lambda'_{\alpha\beta} \cong \frac{\delta v}{\omega_c}e^{-j\omega_c t} \\ \delta i_{\alpha\beta} &= \left(\frac{l_d+l_q}{2\Delta}\cdot\frac{\delta v}{\omega_c}\right)e^{j\omega_c t} \\ &\quad - \frac{\delta v}{\omega_c}\sqrt{\left(\frac{l_d-l_q}{2\Delta}\right)^2 + \left(\frac{l_{dq}}{\Delta}\right)^2}\, e^{j(2\vartheta+\varepsilon-\omega_c t)} \\ &\quad \text{for } l_d > l_q. \end{aligned} \tag{8, 9}$$

Equation (9) shows that cross saturation introduces on ϑ an error equal to $\varepsilon/2$ since the angle $(2\vartheta+\varepsilon)$ is effectively tracked.

A similar situation occurs when a sinusoidal pulsating signal is injected instead of the rotating one. If a sinusoidal voltage (flux) is injected, the corresponding sinusoidal current is detected, and the angle ψ is tracked for which both $\delta\lambda_{dq}$ and δi_{dq} vectors have the same direction. This situation can be imposed from (5) by substituting

$$\delta i_{dq} = \delta i\ e^{j\psi} \quad \delta\lambda_{dq} = \delta\lambda\ e^{j\psi} \quad \delta\lambda'_{dq} = \delta\lambda\ e^{-j\psi}. \tag{10}$$

Thus, (11) is obtained, i.e.,

$$\frac{\delta i}{\delta\lambda} = \frac{l_d+l_q}{2\Delta} - \sqrt{\left(\frac{l_d-l_q}{2\Delta}\right)^2 + \left(\frac{l_{dq}}{\Delta}\right)^2}\cdot e^{j\varepsilon}\cdot e^{-2j\psi} \ \text{ for } \ l_d > l_q \tag{11}$$

where the amplitude and argument of the backward coefficient have been evidenced, as done in (9).

As is shown, (11) is satisfied for $\psi = (\varepsilon/2) \pm k(\pi/2)$, where k is any positive integer. Of course, the d-axis is normally tracked because of the lower $\delta i/\delta\lambda$ ratio.

From this discussion, it can then be concluded that cross saturation introduces an error equal to $\varepsilon/2$ (12) in the ϑ detection, regardless of the rotating or pulsating injected sinusoidal signals, as shown in

$$\text{err} = +\frac{1}{2}\varepsilon. \tag{12}$$

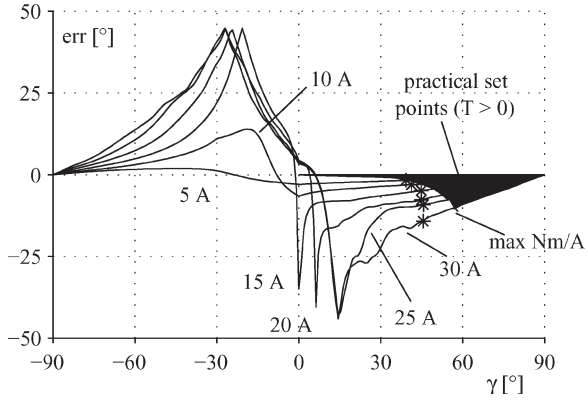

Fig. 6. Error as function of γ for various i amplitudes, where $\gamma = \angle i_{dq}$.

Of course, the error (12) is variable, which depends on the differential inductances and, consequently, on the working point.

Another significant parameter is the ratio of the negative sequence amplitude b over the positive sequence amplitude f, which is given in the following equation regardless of whether (3) or (5) is referred to:

$$\frac{b}{f} = \frac{\sqrt{(l_d-l_q)^2 + 4l_{dq}^2}}{l_d+l_q}. \tag{13}$$

This ratio represents the motor capability of giving useful position information, which in turn depends on the motor anisotropy in the specific working point. However, since the cross-saturation inductance l_{dq} has been introduced, an equivalent anisotropy ratio (ar) has to be defined, as shown in

$$\text{ar} = \frac{1+\frac{b}{f}}{1-\frac{b}{f}}. \tag{14}$$

Let us point out that b/f is always larger than zero; thus, the ar value is larger than one.

Of course, large ar values are welcome. However, ar is a function of the l_d, l_q, and l_{dq} values, which are variable, depending, as usual, on the working point. As a consequence, the effectiveness of the position estimate will also depend on the working point.

Starting from the measured data, such as that of Figs. 2–5, the differential inductances can be estimated at each (i_d, i_q) point. Once l_d, l_q, and l_{dq} are known, the ar value (14) and the error $\varepsilon/2$ (12) can be evaluated at each (i_d, i_q) point.

Fig. 6 shows the error $\varepsilon/2$, as calculated from the characteristics of Figs. 2–5. The error is plotted versus the argument γ of the i_{dq} current vector for some set values of the current amplitude.

As can be seen from Fig. 6, very large errors are possible, up to 45° for specific operating points. The situation may look better only if the practical set points are considered, i.e., the

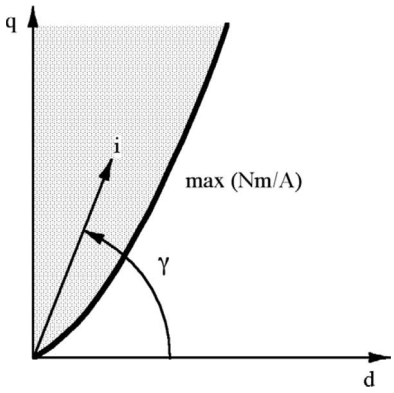

Fig. 7. Practical set points ($T > 0$).

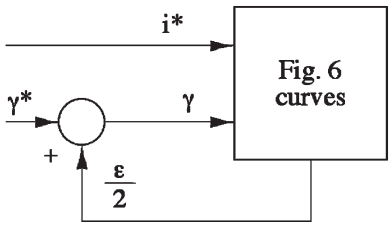

Fig. 8. Effect of angular error on sensorless operation.

area bounded by the q-axis and the maximum torque per ampere curve. This area is evidenced in Fig. 7 (shaded), for motoring ($T > 0$), and corresponds to the larger γ values in Fig. 6. For braking ($T < 0$), the corresponding area is symmetrical with respect to the q-axis. In this area, the error looks limited, at least for not too large current amplitudes.

However, during sensorless operation, with a set γ^* value, the controlled γ value is typically lower than γ^*, due to the orientation error $\varepsilon/2$. In fact, γ must satisfy

$$\gamma = \gamma^* + \frac{\varepsilon(i, \gamma)}{2} \tag{15}$$

which represents the equilibrium point of the feedback shown in Fig. 8.

Equation (15) implies that the effective sensorless operating point is shifted to the left in Fig. 6. In fact, with reference to $T > 0$, the error is negative as the l_{dq} inductance is, and γ results are lower than γ^*. As a consequence, the actual errors are larger than those corresponding to the set γ^*. These are shown in Fig. 6 by the starred points, which correspond to the set max torque per ampere curve points. With reference to Fig. 8, let us also point out that the shown feedback is positive since $\partial\varepsilon/\partial\gamma > 0$, at least in the considered zone (Fig. 6). Unstable operation does not occur in this case since the loop gain is lower than one, at least for the considered current values.

Let us now refer to Fig. 9, where the differential ar is shown in the (i_d, i_q) plane. The ar value is very good in most of the practical working points (Fig. 7). On the contrary, a very critical zone is evidenced near to the (15,0) point, which is far from the practical area. However, near to the no-load point (0,0), the ar values become very low, leading to a possible poor performance when a current ripple is present.

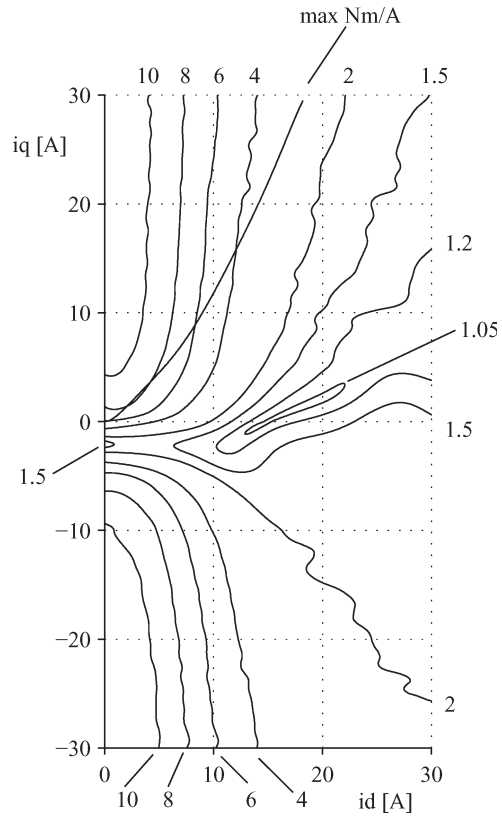

Fig. 9. Constant differential ar in i_d, i_q plane.

III. Experimental Validation

The errors predicted from Fig. 6 have been confirmed by experiment. The IPM motor of Fig. 1 was current controlled, and the i_d and i_q values were freely imposed. The motor was slowly rotated at 100 r/min by a coaxial drive. In addition, a rotating voltage vector was applied at a 400-Hz carrier frequency. The slow rotational speed was chosen to obtain a better spectral separation from rotational and carrier frequencies.

The resulting current backward component was tracked to find out the $(2\tilde{\vartheta} + \varepsilon)$ angle, as suggested in (9). Then, the error $(\tilde{\vartheta} - \vartheta)$ was measured, with ϑ coming from a shaft encoder.

In Figs. 10 and 11, the measured errors are shown when i_q is set to -5 and 10 A, respectively, while i_d is moved linearly from 0 to 20 A. Fig. 12 shows the corresponding calculated errors. As can be seen, a very good accordance is met in both cases. Let us observe that during the tests of Figs. 10 and 11, the applied (rotating) voltage vector was very large, i.e., 75 V. At 400 Hz, it corresponds to a rotating flux vector whose amplitude is 0.03 V · s, which is less than one-tenth of the rated flux. This was done to improve the reliability of the error estimate.

Finally, Figs. 13–16 show the influence of the ar value on the needed carrier voltage amplitude. The same experimental setup that was used in Figs. 10 and 11 has been adopted. The amplitude of the injected (rotating) voltage is varied from 0 to 100 V when the motor is running at 100 r/min. $(\sin 2\tilde{\vartheta})$ and $(\sin 2\vartheta)$ signals are shown for some different (i_d, i_q) working points. Of course, when the carrier amplitude is zero, no information is obtained, and the $(\sin 2\tilde{\vartheta})$ signal is corrupted by noise. The noise vanishes in a way that depends on the local anisotropy.

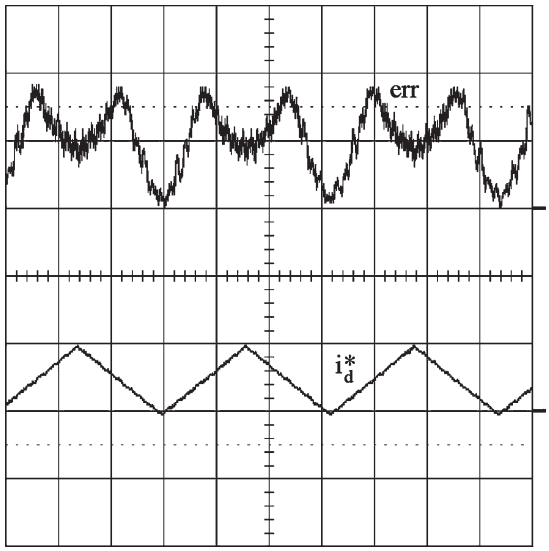

Fig. 10. Measured error for $i_q = -5$ A and i_d varied from 0 to 20 A. Measured error: err (25° el/div). Set motor current: i_d^* (20 A/div). Time base 1 s/div.

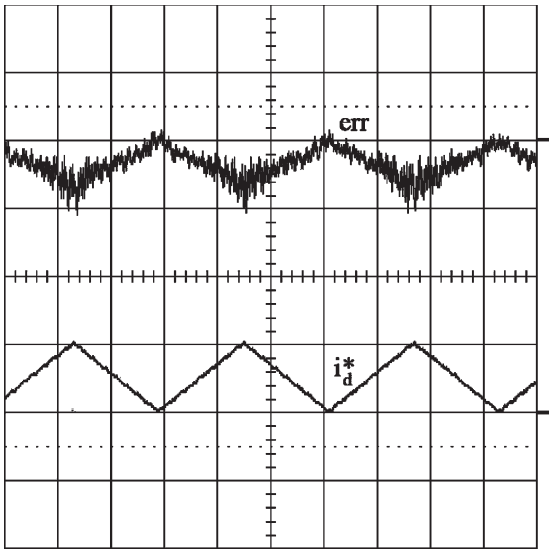

Fig. 11. Measured error for $i_q = 10$ A and i_d varied from 0 to 20 A. Measured error: err (25° el/div). Set motor current: i_d^* (20 A/div). Time base 1 s/div.

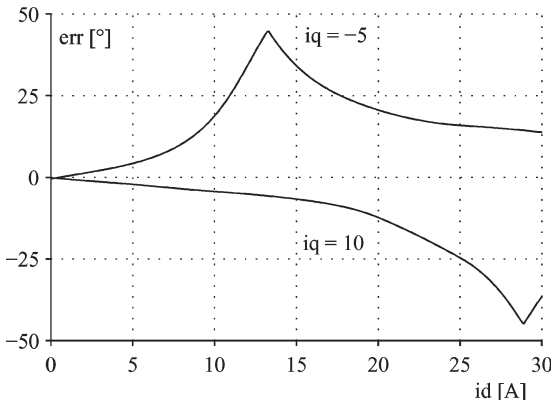

Fig. 12. Calculated error as a function of i_d for $i_q = -5$ and 10 A.

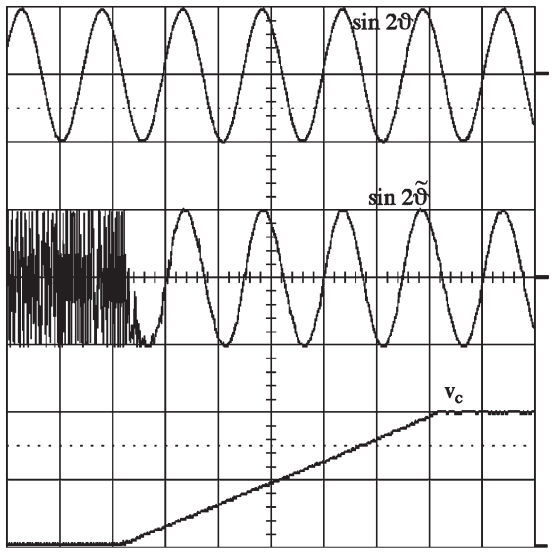

Fig. 13. Estimated angle $(\sin 2\tilde{\vartheta})$ for injected carrier voltage v_c increased from 0 to 100 V ($i_d = 0$ A, $i_q = 0$ A). Exciting (rotating) voltage: v_c (50 V/div). Time base: 100 ms/div.

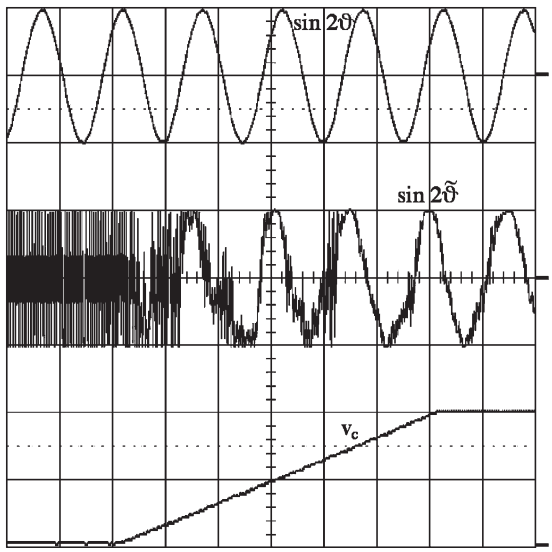

Fig. 14. Estimated angle $(\sin 2\tilde{\vartheta})$ for injected carrier voltage v_c increased from 0 to 100 V ($i_d = 15$ A, $i_q = 0$ A). Exciting (rotating) voltage: v_c (50 V/div). Time base: 100 ms/div.

Let us observe that no particular care was taken in maximizing the signal-to-noise ratio. In particular, the effect of inverter deadtime and delays was not compensated at all. This was done for simplicity since the main goal was verification of the sensitivity of the angle estimate to the motor working points.

Fig. 13 refers to the no-load point $(i_d = 0, i_q = 0)$. As is shown, the angle estimate is very good even for low values of the injected voltage. In fact, in this case, the ar value is near to 6 (Fig. 9). Figs. 15 and 16 show a similar situation for other two points where the ar value is good. Fig. 15 refers to a point (10,12) on the max torque per ampere locus, while Fig. 16 is related to a flux-weakened situation (5,15). On the contrary, Fig. 14 shows that the point $(i_d = 15, i_q = 0)$ does not lead to a reliable estimate even if a very large voltage is applied.

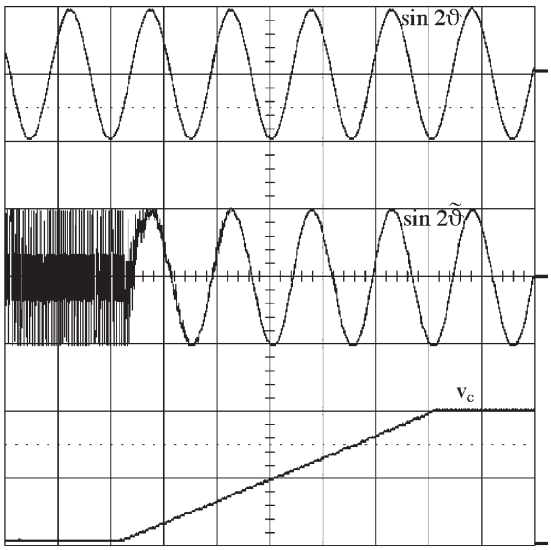

Fig. 15. Estimated angle $(\sin 2\tilde{\vartheta})$ for injected carrier voltage v_c increased from 0 to 100 V ($i_d = 10$ A, $i_q = 12$ A). Exciting (rotating) voltage: v_c (50 V/div). Time base: 100 ms/div.

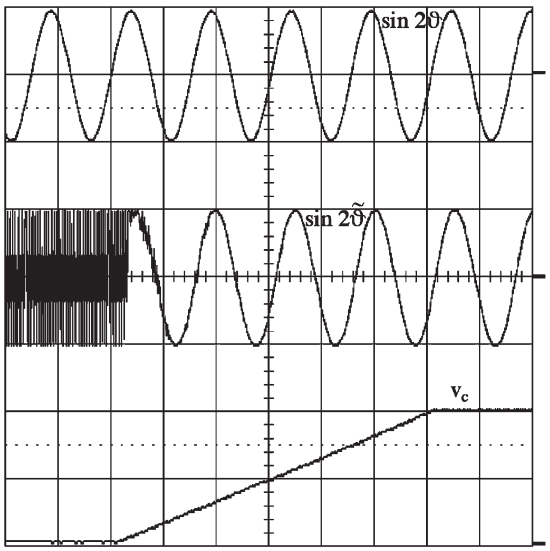

Fig. 16. Estimated angle $(\sin 2\tilde{\vartheta})$ for injected carrier voltage v_c increased from 0 to 100 V ($i_d = 5$ A, $i_q = 15$ A). Exciting (rotating) voltage: v_c (50 V/div). Time base: 100 ms/div.

In fact, in this case, Fig. 9 shows that the corresponding ar value is practically one and the negative sequence component practically vanishes.

In conclusion, the impact of cross saturation on sensorless control predicted by the analysis has been fully confirmed by experiment.

IV. Conclusion

This paper has pointed out that cross saturation has a sensible effect on the conventional sensorless position detection based on injection of a carrier frequency.

The resulting orientation error is inherent to the machine magnetic behavior and does not depend on the signal injection strategy. It has been shown that this error can rise up to some tenths of degrees depending on the motor loading. As a consequence, compensation for this error is mandatory if an accurate control action is desired.

Due to the inherent nature of this error, a compensation strategy must rely on a very accurate modeling of the motor magnetic behavior, at least at low speed. Of course, at high speed, the control action could refer to the EMF estimation, which is not affected by this phenomenon.

An example of control strategy including compensation of the cross-saturation effect is given in [25], where signal injection and EMF estimation are smoothly combined, leading to a full-speed-range control structure that is particularly suited when a large constant power speed range is present.

References

[1] M. Schroedl and P. Weinmeier, "Sensorless control of reluctance machines at arbitrary operating conditions including standstill," *IEEE Trans. Power Electron.*, vol. 9, no. 2, pp. 225–231, Mar. 1994.

[2] P. L. Jansen and R. D. Lorenz, "Transducerless position and velocity estimation in induction and salient ac machines," *IEEE Trans. Ind. Appl.*, vol. 31, no. 2, pp. 240–247, Mar.-Apr. 1995.

[3] J. Holtz, "State of the art of controlled ac drives without speed sensor," in *Proc. Int. Conf. Power Electron. Drive Syst.*, 1995, vol. 1, pp. 1–6.

[4] K. Rajashekara, A. Kawamura, and K.Matsuse, Eds., *Sensorless Control of ac Motor Drives: Speed and Position Sensorless Operation*, New York: IEEE, 1996.

[5] F. Blaschke, J. Van der Burgt, and A. Vandenput, "Sensorless direct field orientation at zero flux frequency," in *Proc. IEEE IAS Annu. Meeting*, San Diego, CA, Oct. 7–10, 1996, vol. 1, pp. 189–196.

[6] M. Schroedl, "Sensorless control of ac machines at low speed and standstill based on the "INFORM" method," in *Proc. IEEE IAS Annu. Meeting*, San Diego, CA, Oct. 7–10, 1996, vol. 1, pp. 270–277.

[7] A. Vagati, G. Franceschini, and M. Pastorelli, "High performance control of synchronous reluctance motor," *IEEE Trans. Ind. Appl.*, vol. 33, no. 52, pp. 983–991, Jul.-Aug. 1997.

[8] P. Vas, *Sensorless Vector and Direct Torque Control*. New York: Oxford Univ. Press, 1998. xxxi, 729 p.

[9] A. Vagati, M. Pastorelli, G. Franceschini, and C. Petrache, "Design of low-torque-ripple synchronous reluctance motors," *IEEE Trans. Ind. Appl.*, vol. 34, no. 4, pp. 758–765, Jul.-Aug. 1998.

[10] A. Vagati, M. Pastorelli, G. Franceschini, and V. Drogoreanu, "Flux-observer-based high-performance control of synchronous reluctance motors by including cross saturation," *IEEE Trans. Ind. Appl.*, vol. 35, no. 3, pp. 597–605, May-Jun. 1999.

[11] S. Ogasawara and H. Akagi, "Implementation and position control performance of a position-sensorless IPM motor drive system based on magnetic saliency," *IEEE Trans. Ind. Appl.*, vol. 34, no. 4, pp. 806–812, Jul.-Aug. 1998.

[12] S.-J. Kang, J.-I. Ha, and S.-K. Sul, "Position controlled synchronous reluctance motor without rotational transducer," in *Proc. IEEE 33rd IAS Annu. Meeting*, 1998, vol. 1, pp. 671–676.

[13] M. J. Corley and R. D. Lorenz, "Rotor position and velocity estimation for a salient-pole permanent magnet synchronous machine at standstill and high speeds," *IEEE Trans. Ind. Appl.*, vol. 34, no. 4, pp. 784–789, Jul.-Aug. 1998.

[14] M. D. Manjrekar, T. A. Lipo, S. C. G. Chang, and K. S. Kim, "Flux tracking methods for direct field orientation," in *Proc. ICEM*, Turkey, Sep. 1998, pp. 1022–1029.

[15] J. Holtz, "Sensorless position control of induction motors–An emerging technology," *IEEE Trans. Ind. Electron.*, vol. 45, no. 6, pp. 840–851, Dec. 1998.

[16] J. I. Ha and S. K. Sul, "Sensorless filed orientation control of an induction machine by high frequency signal injection," *IEEE Trans. Ind. Appl.*, vol. 35, no. 1, pp. 45–51, Jan./Feb. 1999.

[17] A. Consoli, F. Russo, G. Scarcella, and A. Testa, "Low and zero speed sensorless control of synchronous reluctance motors," *IEEE Trans. Ind. Appl.*, vol. 35, no. 5, pp. 1050–1057, Sep.-Oct. 1999.

[18] M. W. Degner and R. D. Lorenz, "Position estimation in induction machines utilizing rotor bar slot harmonics and carrier-frequency signal injection," *IEEE Trans. Ind. Appl.*, vol. 36, no. 3, pp. 736–742, May-Jun. 2000.

[19] A. Vagati, M. Pastorelli, F. Scapino, and G. Franceschini, "Impact of cross saturation in synchronous reluctance motors of the transverse-laminated type," *IEEE Trans. Ind. Appl.*, vol. 36, no. 4, pp. 1039–1046, Jul./Aug. 2000.
[20] A. Vagati, A. Canova, M. Chiampi, M. Pastorelli, and M. Repetto, "Design refinement of synchronous reluctance motors through finite-element analysis," *IEEE Trans. Ind. Appl.*, vol. 36, no. 4, pp. 1094–1102, Jul./Aug. 2000.
[21] A. Consoli, G. Scarcella, G. Tutino, and A. Testa, "Sensorless field oriented control using common mode currents," in *Proc. IEEE-IAS Annu. Meeting*, Roma, Italy, Oct. 8–12, 2000, pp. 1866–1873.
[22] A. Vagati, M. Pastorelli, P. Guglielmi, and E. Capecchi, "Position sensorless control of transverse-laminated synchronous reluctance motors," *IEEE Trans. Ind. Appl.*, vol. 36, no. 3, pp. 736–742, May-Jun. 2001.
[23] R. D. Lorenz, "Practical issues and research opportunity when implementing zero-speed sensorless control," in *Proc. 5th ICEMS*, Aug. 18–20, 2001, vol. 1, pp. 1–10.
[24] J. Holtz, "Sensorless control of induction motor drives," *Proc. IEEE*, vol. 90, no. 8, pp. 1359–1394, Aug. 2002.
[25] A. Vagati, P. Guglielmi, M. Pastorelli, and G. Pellegrino, "Position-sensorless control of permanent-magnet-assisted synchronous reluctance motor," *IEEE Trans. Ind. Appl.*, vol. 40, no. 2, pp. 615–622, Mar./Apr 2004.

Paolo Guglielmi was born in Imperia, Italy, in 1970. He received the M.Sc. degree in electronic engineering and the Ph.D. degree in electrical engineering from the Politecnico di Torino, Turin, Italy, in 1996 and 2001, respectively.

In 1997, he joined the Dipartimento di Ingegneria Elettrica, Politecnico di Torino, where he became a Researcher in 2002. He has authored several papers published in technical journals and conference proceedings. His fields of interest include power electronics, high-performance servo drives, and computer-aided design of electrical machines.

Dr. Guglielmi is a registered professional engineer in Italy.

Michele Pastorelli (M'05) was born in Novara, Italy, in 1962. He received the Laurea and Ph.D. degrees in electrical engineering from the Politecnico di Torino, Turin, Italy, in 1987 and 1992, respectively.

In 1988, he joined the Dipartimento di Ingegneria Elettrica, Politecnico di Torino, where he is currently an Associate Professor. He has authored or coauthored more than 70 papers published in technical journals and conference proceedings. His fields of interest include power electronics, high-performance servo drives, and energetic behaviors of electrical machines.

Dr. Pastorelli is a registered professional engineer in Italy.

Alfredo Vagati (M'88–SM'92–F'98) received the Laurea degree in electrical engineering from the Politecnico di Torino, Turin, Italy, in 1970.

After a few years working in industry with Olivetti, he joined the Politecnico di Torino, in 1975, as an Assistant Professor. From 1982 to 1990, he was an Associate Professor of electrical drives. In 1990, he became a Professor of electrical machines and drives with the University of Cagliari, Cagliari, Italy. In 1991, he rejoined the Politecnico di Torino in the same capacity. He chaired the Department of Electrical Engineering, Politecnico di Torino, from 1995 to 2003. He has authored or coauthored more than 90 technical papers. His scientific activity, in the field of electrical machines and drives, has focused mainly on high-performance ac drives. He has been involved in several industrial projects in the field of ac drives, as both a designer and a scientific reference. His most important activity concerns design and control of newly developed high-performance synchronous reluctance motors. He has led several countrywide and European research projects in the field of design and control of synchronous-machine-based drives for different applications, including home appliances and the automotive world.

Dr. Vagati is a permanent member of the Technical Program Committee of the Power Conversion and Intelligent Motion, International Conference and Exhibition.